Electronic Supplementary Information (ESI)

Regulation of the surface activity of carbon anodes for rationalization of potassium storage

Xiaozhi Yuan [a, #], Yuli Xiong [b, #], Yu Liu [a], Xijun Wei [a*], Feng Wei [c*], Menglei Wang [d], Yang Cao [a], Gang Tao [a], Qingchun Zhang [a], Qi Wan [a] and Yingze Song [a*]

[a] State Key Laboratory of Environmental-Friendly Energy Materials, Tianfu Institute of Research and Innovation, School of Materials and Chemistry, Southwest University of Science and Technology, Mianyang, Sichuan 621010, P. R. China.
[b] College of Physics and Electronic Engineering, Chongqing Normal University, Chongqing 401331, P. R. China.
[c] School of Materials and Chemical Engineering, Chuzhou University, Chuzhou 239000, P.R. China.
[d] College of Energy, Soochow Institute for Energy and Materials Innovations, Key Laboratory of Advanced Carbon Materials and Wearable Energy Technologies of Jiangsu Province, Soochow University, Suzhou 215006, China.

Corresponding authors: xijunwei1992@swust.edu.cn (X. Wei), fengw@chzu.edu.cn (F. Wei), yzsong@swust.edu.cn (Y. Song).

Keywords: temperature regulation, carbonaceous materials, intrinsic carbon defect, potassium storage

1. Experimental

1.1 *Material preparations*

The HICS products were prepared by employing MgO template route as well as annealing procedure. Typically, 6 g MgO and 6 g naphthalene were evenly mixed in a mortar. Subsequently, the mixed powder was transferred into a porcelain boat. The porcelain boat was first heated at a heating rate of 2 °C/min to 80 ^{o}C for 0.5 h and followed by continuing heating at higher temperature (800, 900 and 1000 ^{o}C, respectively) for 1 h at a heating rate of 5 °C/min and under an Ar atmosphere. The collected samples were etched with H_2SO_4 (0.1 M) for 24 h. Then the as-achieved powders were washed with deionized water until the filtrates were neutral and then dried at 110 ^{o}C for 24 h. The as-obtained samples were grinded and sifted by virtue of a 325-mesh sifter.

1.2 *Material characterizations*

The X-ray diffraction (XRD, Bruker D Advance) was employed to determine the crystal structure of the samples and XRD patterns of HICS were obtained at a scan rate of 5 °/min and a scan range of 10-80 ° under Cu-Kα radiation at 40 KV. Transmission electron microscopy (TEM, JEOL JEM-2100F) with selected area electron diffraction (SAED), field emission scanning electron microscopy (FESEM, ZEISS Sigma 300) were used to characterize the morphology and microstructure. TEM and SEAD obtain micro-regional structural features by projecting an electron beam as a light source onto HICS at an accelerating voltage of 200 KV, and SEM was used to obtain micro-morphology by bombarding the sample with secondary electrons at an accelerating voltage of 10-20 KV to excite the physical information of the sample. The surface valences and chemical compositions were characterized by using the X-ray photoelectron spectrometer (XPS, Thermo Scientific K-Alpha) and the Raman spectrometer (Renishaw inVia), and electron paramagnetic resonance (EPR) measurement (JESFA200). XPS irradiates the HICS surface by Al Kα X-ray as a ray source, interacting with the surface atoms and obtaining the surface valence and composition by full spectrum testing. Raman selected 514.5 nm as the laser wavelength of the argon ion laser, 1800 g/mm for the grating, and the signal was collected by the detector. EPR applied microwaves of frequency υ to the sample in a direction perpendicular to the magnetic field B0. When hυ = gβB0, the unpaired electrons absorb the microwave energy and the EPR pattern is obtained. The adsorption-desorption isotherm of N_2 was obtained by using a Micromeritics 3Flex analyzer. The test results

were obtained at a degassing temperature of 200 °C and for 8 h.

1.3 ***Electrochemical measurements***

The working electrode was prepared by mixing the as-obtained HICS, Super P and poly (vinylidene fluoride) (PVDF) with the mass ratio of 5:2:3 at high speed for 30 min, with the N-methyl-2-pyrrolidone (NMP, 99.9%) as the solvent. Then the slurry was coated on the copper foil for the electrode preparation. The vacuum oven was employed to dry the as-prepared electrode at 60 ^{o}C for 8 h. The CR2032 cell was assembled in an Ar-filled glove box filled with high purity argon gas (H_2O < 0.01 ppm, O_2 < 0.01 ppm). The glass fiber membrane (Whatman, GF/D) and potassium foil were used as the separator and counter electrode, respectively. The electrolyte consisted of 0.8 M KPF6 (DEC:EC =1:1 by volume). Cyclic voltammetry (CV) and electrochemical impedance spectroscopy (EIS) tests were conducted by using a Vertex.One electrochemical workstation. An NEWARE automatic battery test system was used to test the rate and cycling performance of PIBs. All PIBs were first activated for 3 cycles at 10 mA g^{-1}. Galvanostatic intermittent titration technique (GITT) measurements were performed on an electrochemical testing equipment (LANHE M340A) with a current pulse of 0.2 A g^{-1} for 10 mins, followed by a relaxation time of 30 mins to reach equilibrium potential.

2. Figures

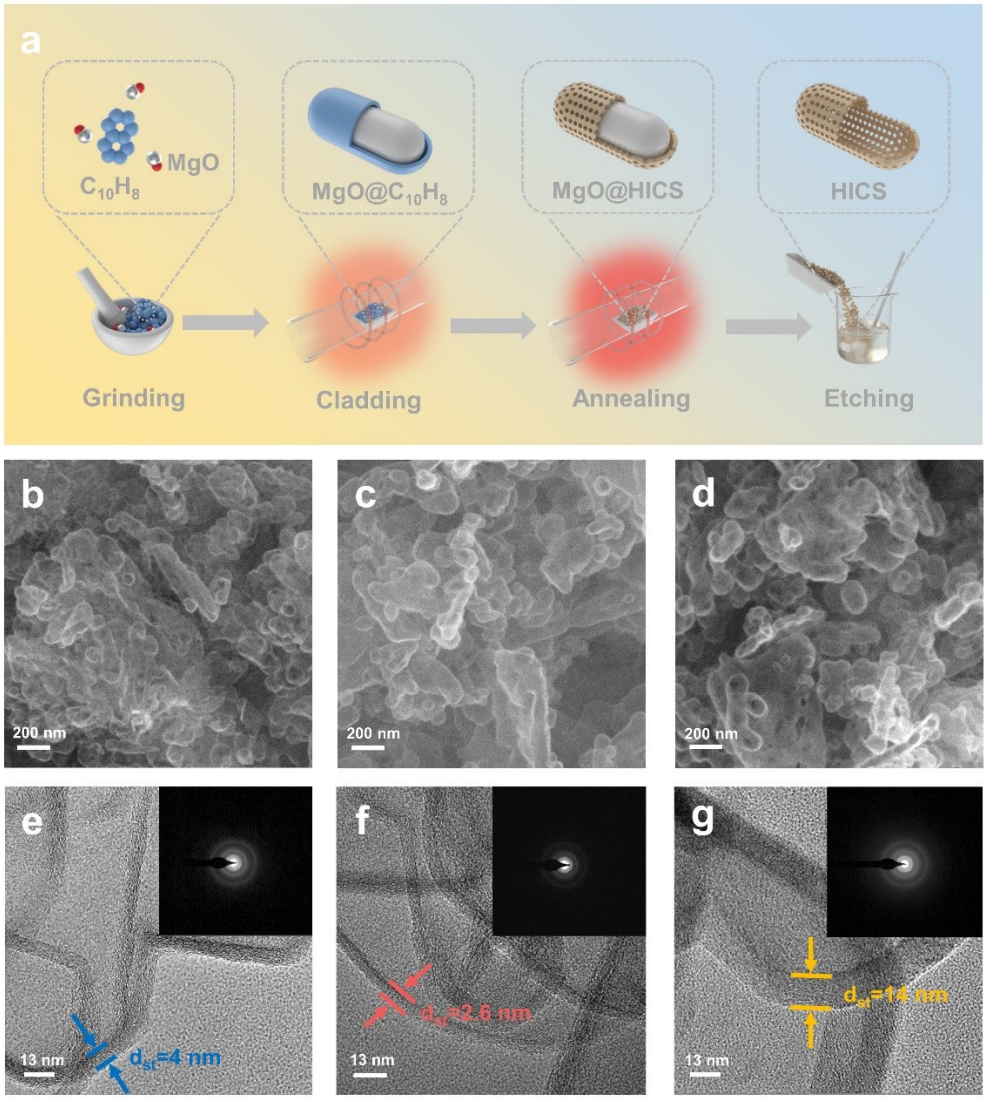

Fig. S1 (a) Schematic illustration of the preparation of HICS. SEM images of (b) HICS-800, (c) HICS-900, (d) HICS-1000, respectively. High-resolution TEM image and SEAD inset of (e) HICS-800, (f) HICS-900, (g) HICS-1000, respectively.

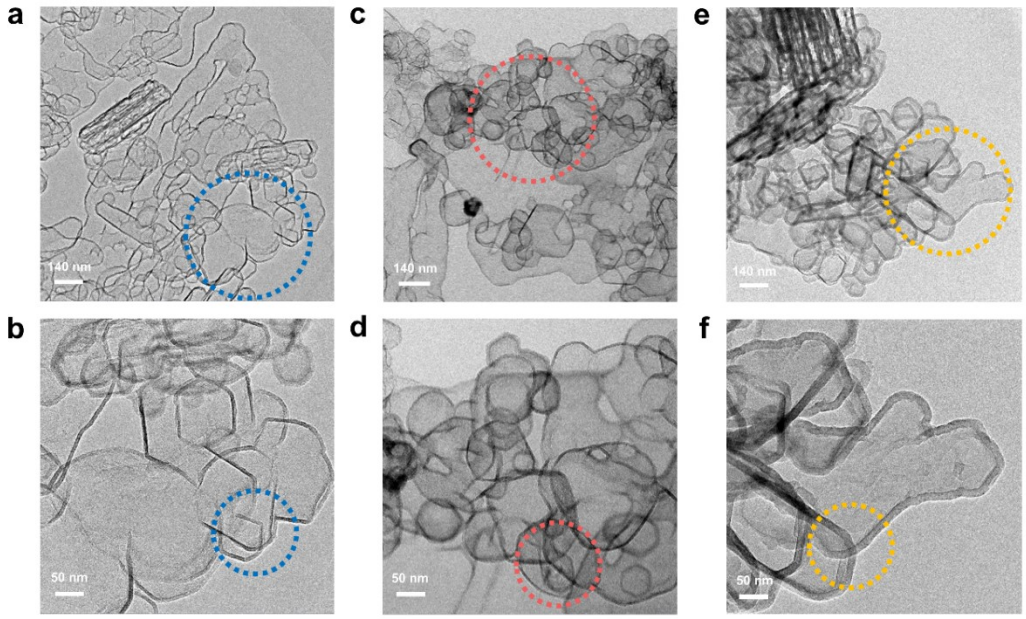

Fig. S2 TEM images of (a–b) HICS-800, (c–d) HICS-900, (e–f) HICS-1000.

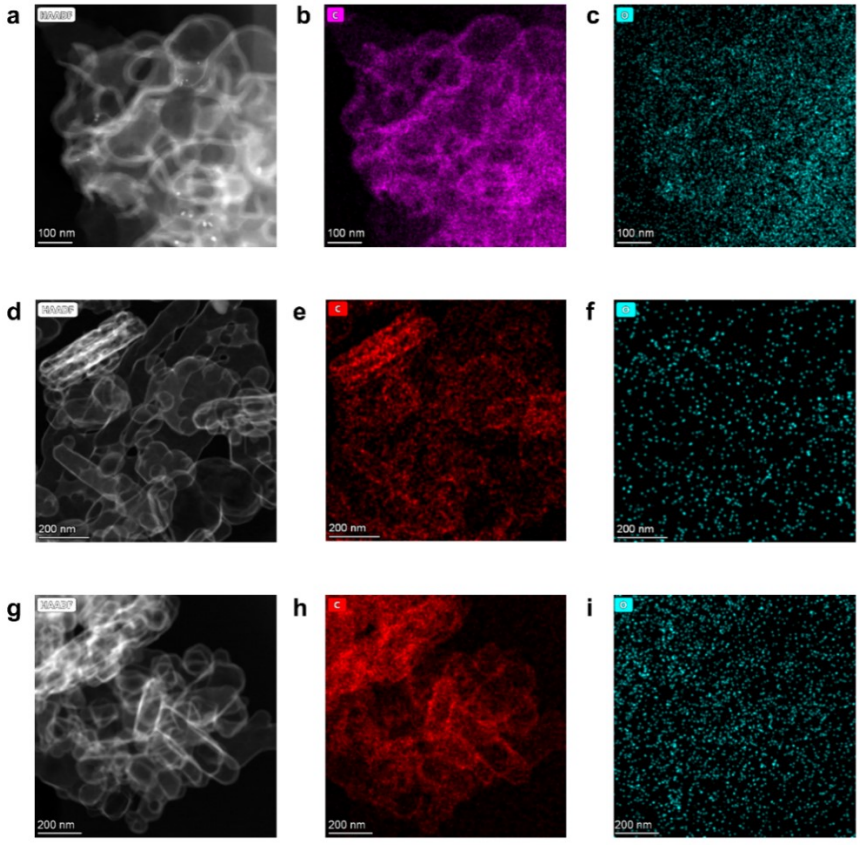

Fig. S3 STEM and EDS map images of (a–c) HICS-900, (d–f) HICS-800 and (g–i) HICS-1000.

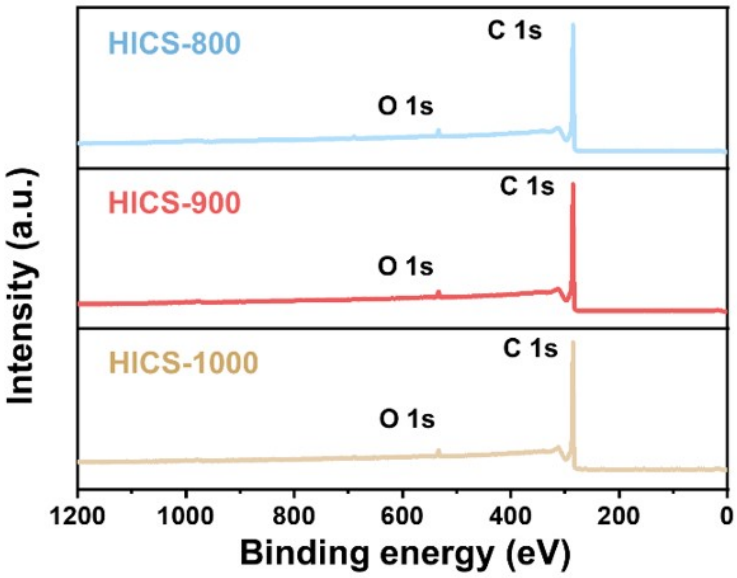

Fig. S4 XPS survey spectra of HICS samples.

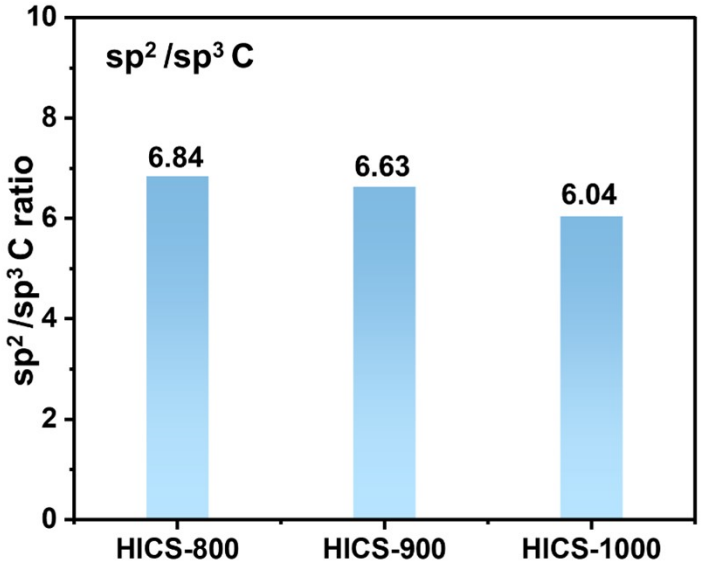

Fig. S5 sp^2/sp^3 C ratio of HICS-800/900/1000.

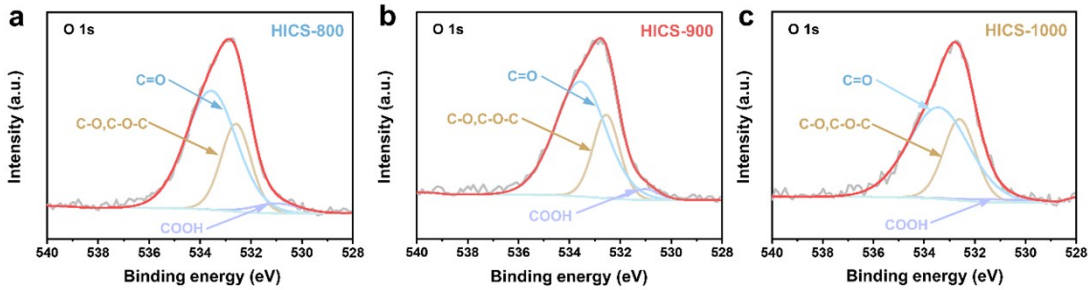

Fig. S6 High-resolution O 1s spectra of (a) HICS-800, (b) HICS-900 and (c) HICS-1000.

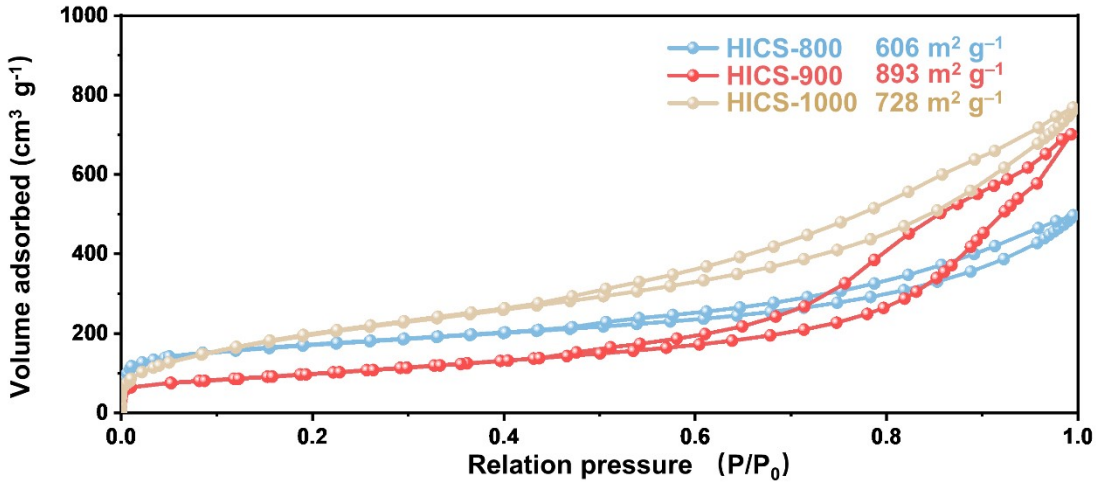

Fig. S7 Nitrogen adsorption-desorption isothermal curves of HICS-800/900/1000.

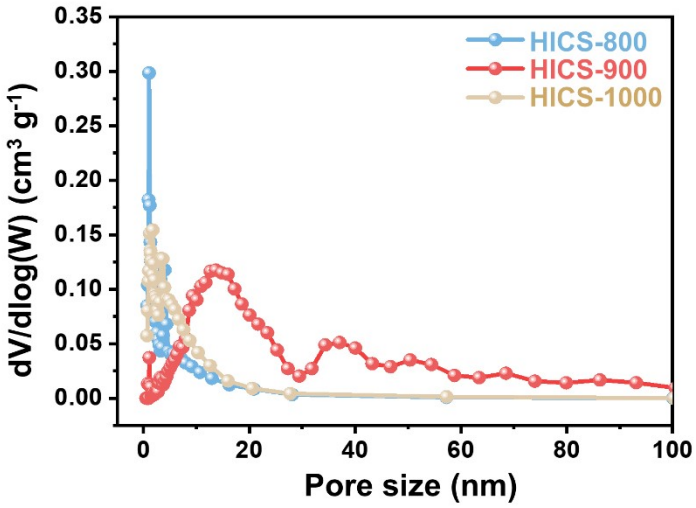

Fig. S8 Pore size distribution of HICS samples.

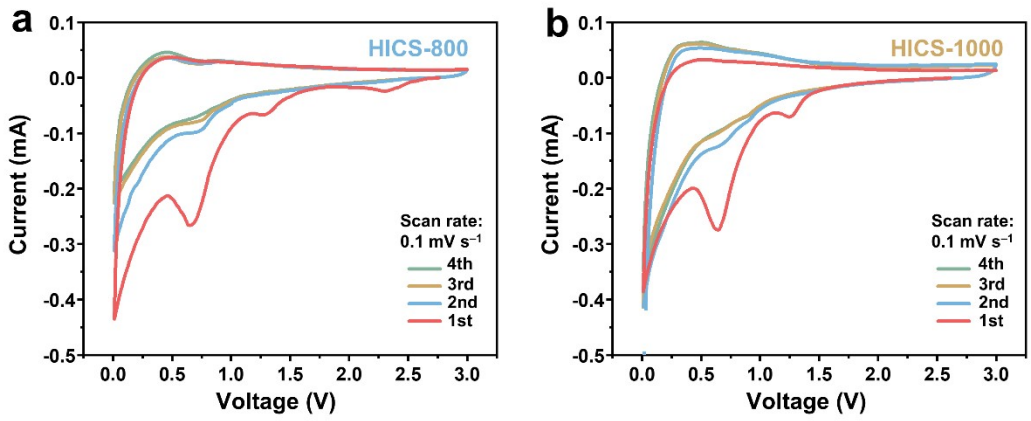

Fig. S9 CV curves for (a) HICS-800, (b) HICS-1000 anodes during the first four cycles for a scan rate range of 0.1 mV s^{-1}.

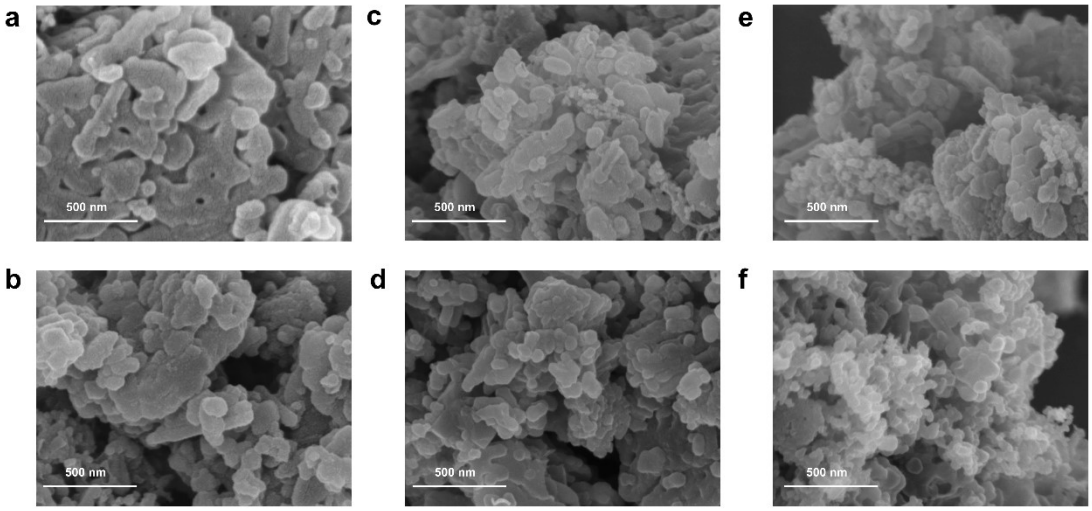

Fig. S10 SEM images of (a) HICS-800 before cycle, (b) HICS-800 after cycle, (c) HICS-900 before cycle, (d) HICS-900 after cycle, (e) HICS-1000 before cycle, (f) HICS-1000 after cycle.

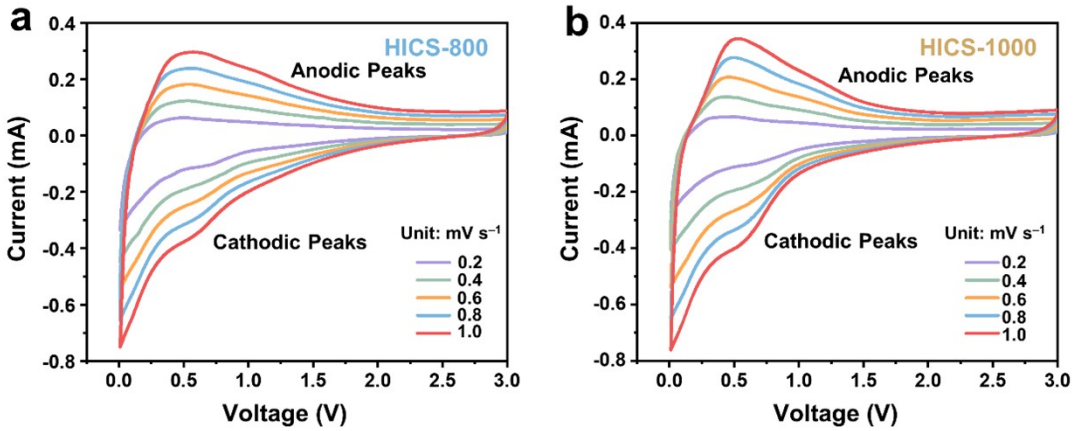

Fig. S11 CV curves of (a) HICS-800, (b) HICS-1000 anode at scan rate range of 0.2 to 1.0 mV s^{-1}

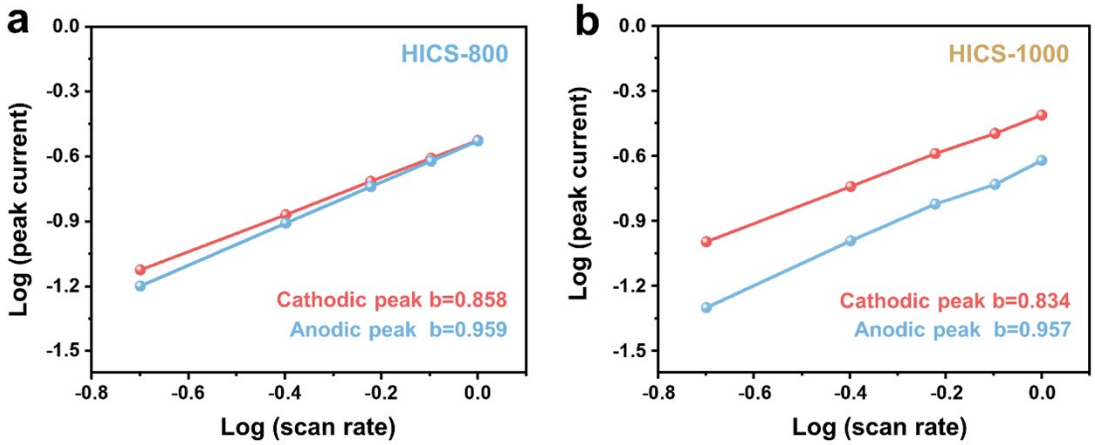

Fig. S12 b value determination of (a) HICS-800, (b) HICS-1000 based on the anodic and cathodic peaks.

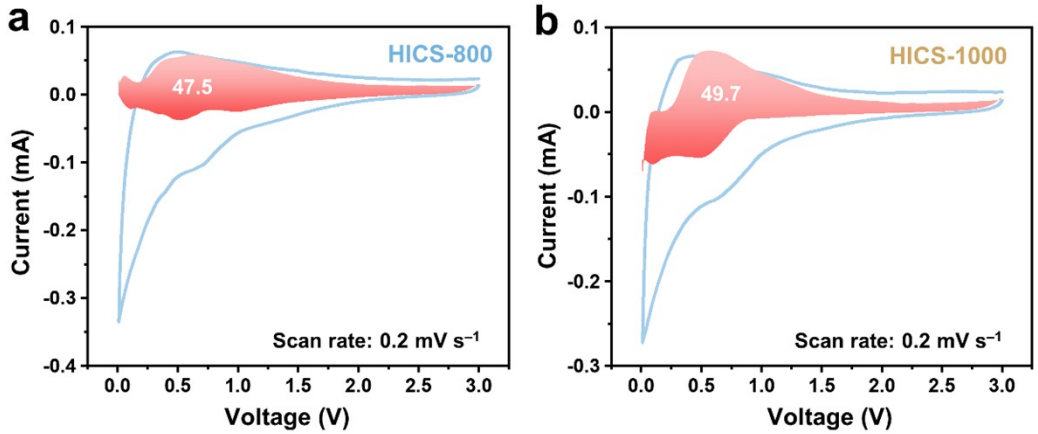

Fig. S13 Contribution percentages of (a) HICS-800 and (b) HICS-1000 anode at 0.2 mV s^{-1}.

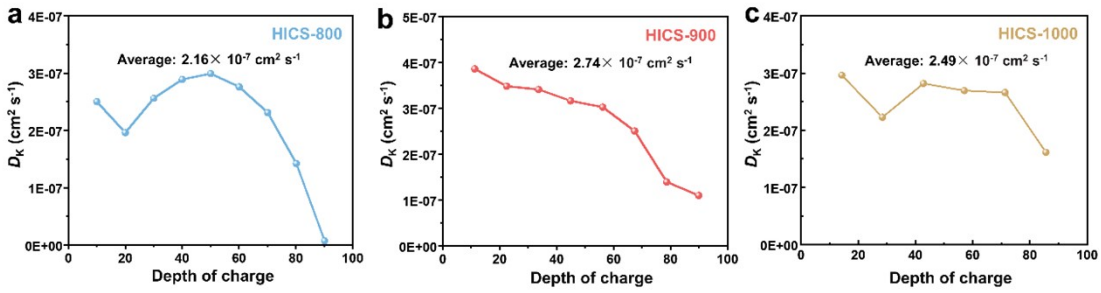

Fig. S14 The potassium-ion diffusion coefficients of (a) HICS-800, (b) HICS-900 and (c) HICS-1000 during the charging process based on the GITT method.

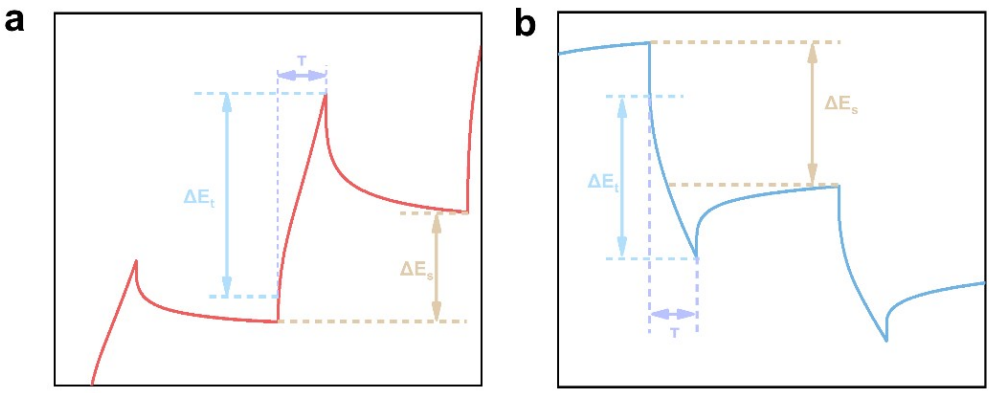

Fig. S15 Schematic representation of the GITT in (a) discharge and (b) charge process.

Note: the diffusion coefficients were calculated based on the second law with the following Equation:

$$D_k = \frac{4L^2}{\pi\tau}\frac{\Delta Es^2}{\Delta E\tau^2}$$

(where τ means the duration of the current pulse, L is electrode thickness. Besides, τ, ΔEs and ΔEτ can be obtained from the GITT curves.)

Table S1. Pseudocapacitance contribution of HICS-800, HICS-900 and HICS-1000.

Scan rate (mV s^{-1})	0.2	0.4	0.6	0.8	1.0
Sample	Contribution ratio (%)				
HICS-800	47.5	55.7	60.9	63.8	67.0
HICS-900	**51.7**	**58.6**	**64.0**	**67.5**	**70.5**
HICS-1000	49.7	55.8	61.3	65.3	68.8

Table S2. Diffusion coefficient of HICS-800, HICS-900 and HICS-1000 electrodes. Measured with a current pulse of 0.2 A g^{-1} for 600 s followed by 1800 s of relaxation time.

HICS-800 Discharge	**HICS-800 charge**	**HICS-900 Discharge**	**HICS-900 charge**	**HICS-1000 Discharge**	**HICS-1000 charge**
3.82×10^{-07}	**2.50×10^{-07}**	**3.77×10^{-07}**	**3.85×10^{-07}**	**3.71×10^{-07}**	**2.96×10^{-07}**
3.39×10^{-07}	**1.96×10^{-07}**	**3.29×10^{-07}**	**3.48×10^{-07}**	**2.73×10^{-07}**	**2.22×10^{-07}**
2.39×10^{-07}	**2.56×10^{-07}**	**2.31×10^{-07}**	**3.41×10^{-07}**	**2.17×10^{-07}**	**2.81×10^{-07}**
2.19×10^{-07}	**2.89×10^{-07}**	**2.28×10^{-07}**	**3.16×10^{-07}**	**1.97×10^{-07}**	**2.69×10^{-07}**
1.79×10^{-07}	**2.99×10^{-07}**	**1.94×10^{-07}**	**3.02×10^{-07}**	**1.66×10^{-07}**	**2.66×10^{-07}**
1.64×10^{-07}	**2.76×10^{-07}**	**1.60×10^{-07}**	**2.50×10^{-07}**	**1.38×10^{-07}**	**1.61×10^{-07}**
1.29×10^{-07}	**2.31×10^{-07}**	**1.19×10^{-07}**	**1.39×10^{-07}**	**9.66×10^{-08}**	
9.61×10^{-08}	**1.42×10^{-07}**	**8.93×10^{-08}**	**1.09×10^{-07}**	**4.96×10^{-08}**	
6.24×10^{-08}	**7.16×10^{-09}**	**4.92×10^{-08}**		**3.84×10^{-08}**	
3.60×10^{-08}		**4.43×10^{-08}**		**1.93×10^{-08}**	
2.22×10^{-08}		**3.03×10^{-08}**		**1.30×10^{-08}**	
1.91×10^{-08}		**1.87×10^{-08}**			
1.34×10^{-08}		**1.32×10^{-08}**			
5.42×10^{-09}					
Average diffusion coefficient (D_K)					
1.36×10^{-07}	**2.16×10^{-07}**	**1.45×10^{-07}**	**2.74×10^{-07}**	**1.43×10^{-07}**	**2.49×10^{-07}**